

Searches for Prompt Light Gravitino Signatures in e^+e^- Collisions at $\sqrt{s} = 189$ GeV

The OPAL Collaboration

Abstract

Searches for final states expected in models with light gravitinos have been performed, including experimental topologies with multi-leptons with missing energy, leptons and photons with missing energy, and jets and photons with missing energy. No excess over the expectations from the Standard Model has been observed. Limits are placed on production cross-sections in the different experimental topologies. Additionally, combining with searches for the anomalous production of lepton and photon pairs with missing energy, results are interpreted in the context of minimal models of gauge mediated SUSY breaking. Exclusion limits at the 95% confidence level on the supersymmetric particle masses of $m_{\tilde{\ell}} > 83$ GeV and $m_{\tilde{\chi}_1^0} > 85$ GeV for $\tan\beta = 2$, and $m_{\tilde{\tau}} > 69$ GeV, $m_{\tilde{e},\tilde{\mu}} > 88$ GeV and $m_{\tilde{\chi}_1^0} > 76$ GeV for $\tan\beta = 20$, are established.

(Submitted to Phys. Lett. B.)

The OPAL Collaboration

G. Abbiendi², K. Ackerstaff⁸, C. Ainsley⁵, P.F. Akesson³, G. Alexander²², J. Allison¹⁶,
 K.J. Anderson⁹, S. Arcelli¹⁷, S. Asai²³, S.F. Ashby¹, D. Axen²⁷, G. Azuelos^{18,a}, I. Bailey²⁶, A.H. Ball⁸,
 E. Barberio⁸, R.J. Barlow¹⁶, J.R. Batley⁵, S. Baumann³, T. Behnke²⁵, K.W. Bell²⁰, G. Bella²²,
 A. Bellerive⁹, S. Bentvelsen⁸, S. Bethke^{14,i}, O. Biebel^{14,i}, I.J. Bloodworth¹, P. Bock¹¹, J. Böhme^{14,h},
 O. Boeriu¹⁰, D. Bonacorsi², M. Boutemour³¹, S. Braibant⁸, P. Bright-Thomas¹, L. Brigliadori²,
 R.M. Brown²⁰, H.J. Burckhart⁸, J. Cammin³, P. Capiluppi², R.K. Carnegie⁶, A.A. Carter¹³,
 J.R. Carter⁵, C.Y. Chang¹⁷, D.G. Charlton^{1,b}, C. Ciocca², P.E.L. Clarke¹⁵, E. Clay¹⁵, I. Cohen²²,
 O.C. Cooke⁸, J. Couchman¹⁵, C. Couyoumtzelis¹³, R.L. Coxe⁹, M. Cuffiani², S. Dado²¹,
 G.M. Dallavalle², S. Dallison¹⁶, A. de Roeck⁸, P. Dervan¹⁵, K. Desch²⁵, B. Dienes^{30,h}, M.S. Dixit⁷,
 M. Donkers⁶, J. Dubbert³¹, E. Duchovni²⁴, G. Duckeck³¹, I.P. Duerdoth¹⁶, P.G. Estabrooks⁶,
 E. Etzion²², F. Fabbri², M. Fanti², L. Feld¹⁰, P. Ferrari¹², F. Fiedler⁸, I. Fleck¹⁰, M. Ford⁵, A. Frey⁸,
 A. Fürties⁸, D.I. Futyan¹⁶, P. Gagnon¹², J.W. Gary⁴, G. Gaycken²⁵, C. Geich-Gimbel³, G. Giacomelli²,
 P. Giacomelli⁸, D. Glenzinski⁹, J. Goldberg²¹, C. Grandi², K. Graham²⁶, E. Gross²⁴, J. Grunhaus²²,
 M. Gruwé²⁵, P.O. Günther³, C. Hajdu²⁹, G.G. Hanson¹², M. Hansroul⁸, M. Hapke¹³, K. Harder²⁵,
 A. Harel²¹, C.K. Hargrove⁷, M. Harin-Dirac⁴, A. Hauke³, M. Hauschild⁸, C.M. Hawkes¹,
 R. Hawkings²⁵, R.J. Hemingway⁶, C. Hensel²⁵, G. Herten¹⁰, R.D. Heuer²⁵, M.D. Hildreth⁸, J.C. Hill⁵,
 P.R. Hobson²⁵, A. Hocker⁹, K. Hoffman⁸, R.J. Homer¹, A.K. Honma⁸, D. Horváth^{29,c}, K.R. Hossain²⁸,
 R. Howard²⁷, P. Hüntemeyer²⁵, P. Igo-Kemenes¹¹, D.C. Imrie²⁵, K. Ishii²³, F.R. Jacob²⁰,
 A. Jawahery¹⁷, H. Jeremie¹⁸, C.R. Jones⁵, P. Jovanovic¹, T.R. Junk⁶, N. Kanaya²³, J. Kanzaki²³,
 G. Karapetian¹⁸, D. Karlen⁶, V. Kartvelishvili¹⁶, K. Kawagoe²³, T. Kawamoto²³, R.K. Keeler²⁶,
 R.G. Kellogg¹⁷, B.W. Kennedy²⁰, D.H. Kim¹⁹, K. Klein¹¹, A. Klier²⁴, T. Kobayashi²³, M. Kobel³,
 T.P. Kokott³, S. Komamiya²³, R.V. Kowalewski²⁶, T. Kress⁴, P. Krieger⁶, J. von Krogh¹¹, T. Kuhl³,
 M. Kupper²⁴, P. Kyberd¹³, G.D. Lafferty¹⁶, H. Landsman²¹, D. Lanske¹⁴, I. Lawson²⁶, J.G. Layter⁴,
 A. Leins³¹, D. Lellouch²⁴, J. Letts¹², L. Levinson²⁴, R. Liebisch¹¹, J. Lillich¹⁰, B. List⁸, C. Littlewood⁵,
 A.W. Lloyd¹, S.L. Lloyd¹³, F.K. Loebinger¹⁶, G.D. Long²⁶, M.J. Losty⁷, J. Lu²⁷, J. Ludwig¹⁰,
 A. Macchiolo¹⁸, A. Macpherson²⁸, W. Mader³, M. Mannelli⁸, S. Marcellini², T.E. Marchant¹⁶,
 A.J. Martin¹³, J.P. Martin¹⁸, G. Martinez¹⁷, T. Mashimo²³, P. Mättig²⁴, W.J. McDonald²⁸,
 J. McKenna²⁷, T.J. McMahon¹, R.A. McPherson²⁶, F. Meijers⁸, P. Mendez-Lorenzo³¹, F.S. Merritt⁹,
 H. Mes⁷, A. Michelini², S. Mihara²³, G. Mikenberg²⁴, D.J. Miller¹⁵, W. Mohr¹⁰, A. Montanari²,
 T. Mori²³, K. Nagai⁸, I. Nakamura²³, H.A. Neal^{12,f}, R. Nisius⁸, S.W. O’Neale¹, F.G. Oakham⁷,
 F. Odorici², H.O. Ogren¹², A. Oh⁸, A. Okpara¹¹, M.J. Oreglia⁹, S. Orito²³, G. Pásztor^{8,j}, J.R. Pater¹⁶,
 G.N. Patrick²⁰, J. Patt¹⁰, P. Pfeifenschneider¹⁴, J.E. Pilcher⁹, J. Pinfold²⁸, D.E. Plane⁸, B. Poli²,
 J. Polok⁸, O. Pooth⁸, M. Przybycień^{8,d}, A. Quadt⁸, C. Rembser⁸, H. Rick⁴, S.A. Robins²¹,
 N. Rodning²⁸, J.M. Roney²⁶, S. Rosati³, K. Roscoe¹⁶, A.M. Rossi², Y. Rozen²¹, K. Runge¹⁰,
 O. Runolfsson⁸, D.R. Rust¹², K. Sachs⁶, T. Saeki²³, O. Sahr³¹, W.M. Sang²⁵, E.K.G. Sarkisyan²²,
 C. Sbarra²⁶, A.D. Schaile³¹, O. Schaile³¹, P. Scharff-Hansen⁸, S. Schmitt¹¹, M. Schröder⁸,
 M. Schumacher²⁵, C. Schwick⁸, W.G. Scott²⁰, R. Seuster^{14,h}, T.G. Shears⁸, B.C. Shen⁴,
 C.H. Shepherd-Themistocleous⁵, P. Sherwood¹⁵, G.P. Sirolì², A. Skuja¹⁷, A.M. Smith⁸, G.A. Snow¹⁷,
 R. Sobie²⁶, S. Söldner-Rembold^{10,e}, S. Spagnolo²⁰, M. Sproston²⁰, A. Stahl³, K. Stephens¹⁶, K. Stoll¹⁰,
 D. Strom¹⁹, R. Ströhmer³¹, B. Surrow⁸, S.D. Talbot¹, S. Tarem²¹, R.J. Taylor¹⁵, R. Teuscher⁹,
 M. Thiergen¹⁰, J. Thomas¹⁵, M.A. Thomson⁸, E. Torrence⁹, S. Towers⁶, T. Trefzger³¹, I. Trigger⁸,
 Z. Trócsányi^{30,g}, E. Tsur²², M.F. Turner-Watson¹, I. Ueda²³, P. Vannerem¹⁰, M. Verzocchi⁸, H. Voss⁸,
 J. Vossebeld⁸, D. Waller⁶, C.P. Ward⁵, D.R. Ward⁵, P.M. Watkins¹, A.T. Watson¹, N.K. Watson¹,
 P.S. Wells⁸, T. Wengler⁸, N. Wormes³, D. Wetterling¹¹, J.S. White⁶, G.W. Wilson¹⁶, J.A. Wilson¹,
 T.R. Wyatt¹⁶, S. Yamashita²³, V. Zacek¹⁸, D. Zer-Zion⁸

- ¹School of Physics and Astronomy, University of Birmingham, Birmingham B15 2TT, UK
- ²Dipartimento di Fisica dell' Università di Bologna and INFN, I-40126 Bologna, Italy
- ³Physikalisches Institut, Universität Bonn, D-53115 Bonn, Germany
- ⁴Department of Physics, University of California, Riverside CA 92521, USA
- ⁵Cavendish Laboratory, Cambridge CB3 0HE, UK
- ⁶Ottawa-Carleton Institute for Physics, Department of Physics, Carleton University, Ottawa, Ontario K1S 5B6, Canada
- ⁷Centre for Research in Particle Physics, Carleton University, Ottawa, Ontario K1S 5B6, Canada
- ⁸CERN, European Organisation for Nuclear Research, CH-1211 Geneva 23, Switzerland
- ⁹Enrico Fermi Institute and Department of Physics, University of Chicago, Chicago IL 60637, USA
- ¹⁰Fakultät für Physik, Albert Ludwigs Universität, D-79104 Freiburg, Germany
- ¹¹Physikalisches Institut, Universität Heidelberg, D-69120 Heidelberg, Germany
- ¹²Indiana University, Department of Physics, Swain Hall West 117, Bloomington IN 47405, USA
- ¹³Queen Mary and Westfield College, University of London, London E1 4NS, UK
- ¹⁴Technische Hochschule Aachen, III Physikalisches Institut, Sommerfeldstrasse 26-28, D-52056 Aachen, Germany
- ¹⁵University College London, London WC1E 6BT, UK
- ¹⁶Department of Physics, Schuster Laboratory, The University, Manchester M13 9PL, UK
- ¹⁷Department of Physics, University of Maryland, College Park, MD 20742, USA
- ¹⁸Laboratoire de Physique Nucléaire, Université de Montréal, Montréal, Quebec H3C 3J7, Canada
- ¹⁹University of Oregon, Department of Physics, Eugene OR 97403, USA
- ²⁰CLRC Rutherford Appleton Laboratory, Chilton, Didcot, Oxfordshire OX11 0QX, UK
- ²¹Department of Physics, Technion-Israel Institute of Technology, Haifa 32000, Israel
- ²²Department of Physics and Astronomy, Tel Aviv University, Tel Aviv 69978, Israel
- ²³International Centre for Elementary Particle Physics and Department of Physics, University of Tokyo, Tokyo 113-0033, and Kobe University, Kobe 657-8501, Japan
- ²⁴Particle Physics Department, Weizmann Institute of Science, Rehovot 76100, Israel
- ²⁵Universität Hamburg/DESY, II Institut für Experimental Physik, Notkestrasse 85, D-22607 Hamburg, Germany
- ²⁶University of Victoria, Department of Physics, P O Box 3055, Victoria BC V8W 3P6, Canada
- ²⁷University of British Columbia, Department of Physics, Vancouver BC V6T 1Z1, Canada
- ²⁸University of Alberta, Department of Physics, Edmonton AB T6G 2J1, Canada
- ²⁹Research Institute for Particle and Nuclear Physics, H-1525 Budapest, P O Box 49, Hungary
- ³⁰Institute of Nuclear Research, H-4001 Debrecen, P O Box 51, Hungary
- ³¹Ludwigs-Maximilians-Universität München, Sektion Physik, Am Coulombwall 1, D-85748 Garching, Germany

^a and at TRIUMF, Vancouver, Canada V6T 2A3

^b and Royal Society University Research Fellow

^c and Institute of Nuclear Research, Debrecen, Hungary

^d and University of Mining and Metallurgy, Cracow

^e and Heisenberg Fellow

^f now at Yale University, Dept of Physics, New Haven, USA

^g and Department of Experimental Physics, Lajos Kossuth University, Debrecen, Hungary

^h and MPI München

ⁱ now at MPI für Physik, 80805 München

^j and Research Institute for Particle and Nuclear Physics, Budapest, Hungary.

1 Introduction

Supersymmetry (SUSY) provides a method of solving the “naturalness” or “hierarchy” problem by introducing a set of new particles which cancel the large radiative corrections to the Higgs mass. The cancellation is achieved by assuming that, for each Standard Model (SM) particle chirality state, there is one additional particle, identical to its SM partner except that its spin differs by 1/2 unit. If SUSY were an exact symmetry, the new SUSY particles would have the same masses as their SM partners. Since this scenario is experimentally excluded, SUSY must be a broken symmetry. It is typically assumed that SUSY is broken in some “hidden” sector of new particles, and is “communicated” (or mediated) to the “visible” sector of SM and SUSY particles by one of the known interactions. Two scenarios for this mediation have been widely investigated: gravity and gauge mediation. In gauge mediated SUSY breaking (GMSB), the hidden¹ sector can lie at energies as low as about 10^4 GeV. In most current GMSB theoretical work [1, 2, 3], it is assumed that this hidden sector is coupled to a messenger sector, which in turn couples to the visible sector through normal SM gauge interactions. The advantage of GMSB over gravity mediated models is that flavour changing neutral currents cannot be induced by SUSY breaking because the normal gauge interactions are flavour blind. A feature which distinguishes gravity from gauge mediated models is the mass of the gravitino, \tilde{G} . In gravity mediated models, \tilde{G} is usually too heavy to have a significant effect on SUSY phenomenology, while in GMSB models, the \tilde{G} is typically light (< 1 GeV) and is the lightest SUSY particle, the LSP. While \tilde{G} is a spin 3/2 particle, only its spin 1/2 component (which has “absorbed” the goldstino associated with spontaneous SUSY breaking via the “superhiggs” mechanism) interacts with weak, rather than gravitational, strength interactions, and contributes to phenomenology.

The next-to-lightest SUSY particle (NLSP) is usually either the lightest neutralino ($\tilde{\chi}_1^0$) or the lightest scalar lepton ($\tilde{\ell}_1^\pm$), and in a significant fraction of the parameter space the NLSP is the lightest scalar tau lepton ($\tilde{\tau}_1$). The coupling of the SUSY particles to \tilde{G} is small, and typically SUSY particles will decay to the NLSP, which then decays to the gravitino via $\tilde{\chi}_1^0 \rightarrow \gamma \tilde{G}$ or $\tilde{\ell} \rightarrow \ell \tilde{G}$. If the decay to the gravitino occurs with a small lifetime, the distinguishing feature is events with energetic leptons or photons, plus significant missing energy due to the missing gravitinos. OPAL has considered scalar lepton and lightest neutralino pair creation in these scenarios in previous publications [4, 5]. This paper reports the first OPAL results on the systematic search for experimental topologies expected in SUSY models with a light gravitino, assuming prompt decays of the NLSP into the \tilde{G} . It is also possible for the NLSP lifetime to be significant and it may decay near the interaction point, at an observably macroscopic distance, or outside the detector. Many signatures expected with long NLSP lifetimes have been considered in other OPAL publications [4, 6, 7], and the case of arbitrary lifetime will be considered in a subsequent publication. In addition to the new experimental searches which have sensitivity to general SUSY models with light gravitinos, the results reported in this paper are also combined with those from previous publications to constrain minimal GMSB models. Results from searches for GMSB have also been reported by other collaborations [8, 9].

¹In some GMSB papers this is called the “secluded” sector, to avoid confusion with the hidden sector of gravity mediated SUSY breaking models.

2 OPAL Detector and Event Simulation

The OPAL detector is described in detail in Reference [10]. The SUSYGEN [11] event generator was used to simulate most of the signal events. For $\tilde{\chi}_1^0$ pair creation in the $\tilde{\chi}_1^0$ NLSP case, 1000 events were simulated for each $\tilde{\chi}_1^0$ mass, using 6 $m_{\tilde{\chi}_1^0}$ points from 50 GeV to 94 GeV. For $\tilde{\ell}$ pair production in the $\tilde{\chi}_1^0$ NLSP case, 1000 events were generated for each $(m_{\tilde{\ell}}, m_{\tilde{\chi}_1^0})$, using a grid of 48 different points for each $\tilde{\ell}$ flavour. Similar one- or two-dimensional mass grids were used for $\tilde{\ell}$ and $\tilde{\chi}_1^0$ pair production in the $\tilde{\ell}$ (and $\tilde{\tau}$) NLSP cases. For chargino pair production, $\tilde{\chi}_1^+ \tilde{\chi}_1^-$, and the associated pair production of the lightest and second lightest neutralino, $\tilde{\chi}_2^0 \tilde{\chi}_1^0$, in the $\tilde{\chi}_1^0$ NLSP case, the W and Z boson widths can play an important role and are not fully treated in SUSYGEN. The DFGT generator [12] is used to simulate these signal events. It includes spin correlations and allows for a proper treatment of the W boson and the Z boson width effects in the chargino and heavy neutralino decays. Both SUSYGEN and DFGT include initial-state radiation. The JETSET 7.4 package [13] is used for the hadronization. The gravitino mass is set identically to zero in the generation, since a small mass in the range favoured by the models has a negligible effect on the detection efficiencies.

The sources of background include two-photon, lepton-pair, multihadronic, and four-fermion processes. The Monte Carlo generators PHOJET [14] (for $Q^2 < 4.5 \text{ GeV}^2$) and HERWIG [15] (for $Q^2 \geq 4.5 \text{ GeV}^2$) are used to simulate hadronic events from two-photon processes. The Vermaseren [16] program is used to simulate leptonic two-photon processes ($e^+e^-e^+e^-$, $e^+e^-\mu^+\mu^-$ and $e^+e^-\tau^+\tau^-$). Four-fermion processes were simulated using KORALW [17], and with the grc4f [18] generator, both of which take into account all interfering four-fermion diagrams. The improved simulation of the transverse momentum of photons from initial-state radiation makes the use of KORALW essential for events including photons in the final states. Lepton pairs were simulated using the KORALZ [19] generator for $\tau^+\tau^-(\gamma)$, $\mu^+\mu^-(\gamma)$ and $\nu\bar{\nu}\gamma(\gamma)$ events, and the BHWIDE [20] (when both the electron and positron scatter at least 12.5° from the beam axis) and TEEGG [21] (for the remaining phase space) programs for $e^+e^- \rightarrow e^+e^-(\gamma)$ events. Multihadronic, $q\bar{q}(\gamma)$, events were simulated using PYTHIA [13].

Generated signal and background events were processed through the full simulation of the OPAL detector [22] and the same event analysis chain was applied to the simulated events as to the data. A data set of approximately 182 pb^{-1} at a luminosity weighted centre of mass energy of $\sqrt{s} = 188.7 \text{ GeV}$ was used for the analysis.

3 Analysis

For all the selections, after the event reconstruction, double-counting of energy between tracks and calorimeter clusters is corrected by reducing the calorimeter cluster energy by the expected energy deposition from aligned tracks [23]. The selections for events with leptons or hadronic jets plus photons and missing energy described in Section 3.1, as well as four or six leptons plus missing energy in Section 3.2, use the same lepton identification and isolation requirements and preselection as the OPAL Chargino/Neutralino analysis [6]. The most significant preselection cuts require that there is no significant energy in the OPAL forward calorimeters.

3.1 $\tilde{\chi}_1^0$ NLSP

3.1.1 $\tilde{\chi}_1^0 \tilde{\chi}_1^0$ Production with $\tilde{\chi}_1^0$ NLSP

The search for lightest neutralino pair production followed by the decays $\tilde{\chi}_1^0 \rightarrow \gamma \tilde{G}$ uses the OPAL selection of events with photon pairs and missing energy [5]. The analysis selects events with at least two photon candidates and significant missing energy, along with no other significant energy in the event. A total of 24 events are selected, which is consistent with the expectation of 26.9 ± 1.2 events from Standard Model $e^+e^- \rightarrow \nu\bar{\nu}\gamma\gamma(\gamma)$ production and 0.11 ± 0.04 from all other sources. The selection efficiency for $e^+e^- \rightarrow \nu\bar{\nu}\gamma\gamma(\gamma)$ within the kinematic acceptance of the analysis is $(66.4 \pm 2.9)\%$. One can calculate [24] the maximum neutralino mass, $M_{\tilde{\chi}_1^0}^{\max}$, which is consistent with the measured three-momenta of the two photons. A cut on $M_{\tilde{\chi}_1^0}^{\max}$ provides further suppression of the $\nu\bar{\nu}\gamma\gamma(\gamma)$ background while retaining high efficiency for the signal hypothesis. We require that the maximum kinematically allowed mass be greater than $m_{\tilde{\chi}_1^0} - 5$ GeV, which retains $(95.5_{-1.0}^{+2.0})\%$ relative efficiency for signal at all values of $m_{\tilde{\chi}_1^0}$ while suppressing much of the remaining $\nu\bar{\nu}\gamma\gamma(\gamma)$ background. The number of selected events consistent with a given value of $m_{\tilde{\chi}_1^0}$ varies from 14 for $m_{\tilde{\chi}_1^0} \geq 45$ GeV to 3 events at the kinematic limit. The expected number of SM background events decreases from 13.67 ± 0.20 at $m_{\tilde{\chi}_1^0} \geq 45$ GeV to 1.34 ± 0.07 consistent with $m_{\tilde{\chi}_1^0} \geq 94$ GeV.

3.1.2 $\tilde{\ell}^+\tilde{\ell}^-$, $\tilde{\chi}_1^+\tilde{\chi}_1^-$ and $\tilde{\chi}_2^0\tilde{\chi}_1^0$ Production with $\tilde{\chi}_1^0$ NLSP

With a $\tilde{\chi}_1^0$ NLSP, scalar lepton, charginos and neutralinos may be observed via
 $e^+e^- \rightarrow \tilde{\ell}^+\tilde{\ell}^- \rightarrow (\ell^+\tilde{\chi}_1^0)(\ell^-\tilde{\chi}_1^0) \rightarrow (\ell^+\gamma\tilde{G})(\ell^-\gamma\tilde{G})$,
 $e^+e^- \rightarrow \tilde{\chi}_1^+\tilde{\chi}_1^- \rightarrow (W^{(*)+}\tilde{\chi}_1^0)(W^{(*)-}\tilde{\chi}_1^0) \rightarrow (W^{(*)+}\gamma\tilde{G})(W^{(*)-}\gamma\tilde{G})$ and
 $e^+e^- \rightarrow \tilde{\chi}_2^0\tilde{\chi}_1^0 \rightarrow Z^{(*)}\tilde{\chi}_1^0\tilde{\chi}_1^0 \rightarrow (Z^{(*)}\gamma\tilde{G})(\gamma\tilde{G})$.

In all cases, the signature is events with two photons plus missing energy, plus other activity in the detector. Scalar lepton production will always lead to a low multiplicity final state, and only events with at most six tracks are considered in the analysis. Chargino pair production and neutralino associated pair production may lead to either low or high multiplicity final states depending on the decays of the $W^{(*)\pm}$ and $Z^{(*)}$ bosons. For charginos and neutralinos, the analysis is therefore divided into two categories:

- (HM) High-multiplicity topologies, with $N_{\text{ch}} - N_{\text{conv}} > 4$, where N_{ch} is the total number of tracks in the event, and N_{conv} is the number of tracks originating from identified photon conversions,
- (LM) Low-multiplicity topologies, with $N_{\text{ch}} - N_{\text{conv}} \leq 4$.

The background composition depends on the event kinematics, which are functions of the mass difference between the produced particles and the lightest neutralino, $\Delta m = m - m_{\tilde{\chi}_1^0}$. The analysis is therefore separately optimized for different Δm regions, listed in Table 1.

The analyses select events with significant missing energy and two photons. Cuts are applied on the event acoplanarity² (ϕ_{acop}), polar angle of the missing momentum ($\cos\theta_{\text{miss}}$), missing transverse momentum scaled by the beam energy ($p_T^{\text{miss}}/E_{\text{beam}}$) and visible energy scaled by the centre-of-mass energy (E_{vis}/\sqrt{s}). Additionally, unlike other SUSY searches, the LSP gravitino is

²After forcing the event into two jets, the acoplanarity angle is 180° minus the opening angle between the jets in the plane transverse to the beam axis.

essentially massless, and the backgrounds can be further reduced while retaining high efficiency by also imposing a minimum requirement on E_{vis}/\sqrt{s} . In the HM analyses, there is significant background from $e^+e^- \rightarrow W^+W^-$ in some of the kinematic regions. This background is reduced by removing the most energetic photon and forcing the event into two jets, and then cutting on the two-jet mass ($M_{2\text{jet}}$). In the scalar lepton search, it is also required that there be at least one identified, isolated lepton in each event. To maintain a general search, if two leptons are found they are not required to be of the same flavour.

Finally, in all channels, it is required that there be at least two energetic photons in each event. Photons are identified by selecting unassociated clusters in the electromagnetic calorimeter, with the following isolation requirements in a cone centred on the cluster (15° half-angle for the highest energy photon and 10° half-angle for the second photon):

- scalar momentum sum < 1 GeV;
- additional electromagnetic calorimeter energy sum < 5 GeV;
- hadronic calorimeter energy < 5 GeV.

The energies of the most ($E_{\gamma 1}$) and second most ($E_{\gamma 2}$) energetic photon are also used to select signal events.

In the $\tilde{\ell}^+\tilde{\ell}^-$ selections, $\phi_{\text{acop}} > 5^\circ$ is required, while the cut is tightened to $\phi_{\text{acop}} > 10^\circ$ for the $\tilde{\chi}_1^+\tilde{\chi}_1^-$ and $\tilde{\chi}_2^0\tilde{\chi}_1^0$ selections. In all channels, $|\cos\theta_{\text{miss}}| < 0.95$ is required. The values of all other analysis cuts are summarized in Table 1, for the different Δm regions.

Examples distributions of the event visible energy and the energy of the most energetic photon are shown in Figure 1. The selection results are summarized in Table 2, and the numbers of selected events are consistent with Standard Model sources.

The detection efficiencies for events from $\tilde{\ell}^+\tilde{\ell}^-$ production assuming the decays $\tilde{\ell} \rightarrow \ell\tilde{\chi}_1^0$ and $\tilde{\chi}_1^0 \rightarrow \gamma\tilde{G}$ are typically 30–50% for scalar electrons and muons, and 20–40% for scalar tau leptons. Summing the high- and low-multiplicity selections, the detection efficiencies for events from $\tilde{\chi}_1^+\tilde{\chi}_1^-$ production assuming the decays $\tilde{\chi}_1^\pm \rightarrow W^{(*)\pm}\tilde{\chi}_1^0$ and $\tilde{\chi}_1^0 \rightarrow \gamma\tilde{G}$ range from 20–50%, depending on the masses of the chargino and lightest neutralino. Summing the high- and low-multiplicity selections, the detection efficiencies for events from $\tilde{\chi}_2^0\tilde{\chi}_1^0$ production assuming the decays $\tilde{\chi}_2^0 \rightarrow Z^{(*)}\tilde{\chi}_1^0$ and $\tilde{\chi}_1^0 \rightarrow \gamma\tilde{G}$ are typically 20–50%, depending on the mass of the two neutralinos.

3.2 $\tilde{\ell}$ NLSP

3.2.1 $\tilde{\ell}^+\tilde{\ell}^-$ Production with $\tilde{\ell}$ NLSP

The search for lightest scalar lepton pair production followed by the decays $\tilde{\ell}^\pm \rightarrow \ell^\pm\tilde{G}$ uses the OPAL selection of events with lepton pairs and missing energy [4]. The analysis selects events with two lepton candidates and significant missing energy, along with no other significant energy in the event. A total of 301 events were observed in the data, consistent with the 303.3 ± 1.9 events expected from all background sources. A likelihood selection using information about the leptons' energies, charges and polar angles is used to maximize the sensitivity of the analysis to slepton production for each slepton mass. An optimized cut for each scalar lepton mass on the likelihood is applied, as described in Reference [25]. No evidence for anomalous production of lepton pairs with missing energy is observed.

Region		$p_T^{\text{miss}}/E_{\text{beam}}$	E_{vis}/\sqrt{s}	$M_{2\text{jet}}$ (GeV)	$E_{\gamma 1}$ (GeV)	$E_{\gamma 2}$ (GeV)	
$\tilde{\ell}^+\tilde{\ell}^-$							
$3\text{ GeV} < \Delta m < 10\text{ GeV}$		> 0.10	$[0.30, 0.80]$	–	> 15	> 10	
$10\text{ GeV} < \Delta m < m_{\tilde{\ell}}/2$		> 0.08	$[0.40, 0.85]$				
$m_{\tilde{\ell}}/2 < \Delta m < m_{\tilde{\ell}}$			$[0.45, 0.95]$		> 10	> 5	
$\tilde{\chi}_1^+\tilde{\chi}_1^-$							
HM	$3\text{ GeV} < \Delta m < 10\text{ GeV}$	> 0.06	$[0.30, 0.80]$	< 60	> 20	> 3	
	$10\text{ GeV} < \Delta m < m_{\tilde{\chi}^\pm}/2$	> 0.05		–	$[15, 70]$		
	$m_{\tilde{\chi}^\pm}/2 < \Delta m < m_{\tilde{\chi}^\pm} - 20\text{ GeV}$	> 0.04	$[0.40, 0.90]$		$[10, 70]$		
	$m_{\tilde{\chi}^\pm} - 20\text{ GeV} < \Delta m < m_{\tilde{\chi}^\pm}$	> 0.03	$[0.40, 0.95]$		$[5, 50]$		
LM	$3\text{ GeV} < \Delta m < 10\text{ GeV}$	> 0.05	$[0.30, 0.80]$		> 20		
	$10\text{ GeV} < \Delta m < m_{\tilde{\ell}}/2$			$[15, 70]$			
	$m_{\tilde{\chi}^\pm}/2 < \Delta m < m_{\tilde{\chi}^\pm} - 20\text{ GeV}$			$[10, 70]$			
	$m_{\tilde{\chi}^\pm} - 20\text{ GeV} < \Delta m < m_{\tilde{\chi}^\pm}$			$[5, 50]$			
$\tilde{\chi}_2^0\tilde{\chi}_1^0$							
HM	$3\text{ GeV} < \Delta m < 10\text{ GeV}$	> 0.05	$[0.25, 0.75]$	< 50	> 20	> 3	
	$10\text{ GeV} < \Delta m < 30\text{ GeV}$	> 0.04	$[0.30, 0.80]$	< 60			
	$30\text{ GeV} < \Delta m < 80\text{ GeV}$	> 0.035	$[0.40, 0.85]$	–	$[10, 70]$		
	$80\text{ GeV} < \Delta m < M_{\tilde{\chi}_2^0}$	> 0.025	$[0.50, 0.90]$		$[5, 60]$		
LM	$3\text{ GeV} < \Delta m < 10\text{ GeV}$	> 0.05	$[0.25, 0.75]$		> 20		
	$10\text{ GeV} < \Delta m < 30\text{ GeV}$	> 0.04	$[0.30, 0.80]$		$[20, 70]$		
	$30\text{ GeV} < \Delta m < 80\text{ GeV}$	> 0.035	$[0.35, 0.85]$	$[10, 70]$			
	$80\text{ GeV} < \Delta m < M_{\tilde{\chi}_2^0}$	> 0.025	$[0.35, 0.90]$	$[10, 60]$			

Table 1: Analysis requirements on quantities used in the different $\tilde{\chi}_1^0$ NLSP selections.

Channel	Region		data	total bkg.
$\tilde{\ell}^+\tilde{\ell}^-$	$3 \text{ GeV} < \Delta m < 10 \text{ GeV}$		0	1.1 ± 0.2
	$10 \text{ GeV} < \Delta m < m_{\tilde{\ell}}/2$		0	1.3 ± 0.2
	$m_{\tilde{\ell}}/2 < \Delta m < m_{\tilde{\ell}}$		0	2.6 ± 0.4
$\tilde{\chi}_1^+\tilde{\chi}_1^-$	$3 \text{ GeV} < \Delta m < 10 \text{ GeV}$	HM	0	0.6 ± 0.1
		LM	0	1.5 ± 0.4
	$10 \text{ GeV} < \Delta m < m_{\tilde{\chi}^\pm}/2$	HM	3	3.2 ± 0.8
		LM	0	2.1 ± 0.5
	$m_{\tilde{\chi}^\pm}/2 < \Delta m < m_{\tilde{\chi}^\pm} - 20 \text{ GeV}$	HM	4	5.5 ± 1.7
		LM	0	1.4 ± 0.4
	$m_{\tilde{\chi}^\pm} - 20 \text{ GeV} < \Delta m < m_{\tilde{\chi}^\pm}$	HM	5	7.2 ± 3.4
		LM	0	0.8 ± 0.3
$\tilde{\chi}_2^0\tilde{\chi}_1^0$	$3 \text{ GeV} < \Delta m < 10 \text{ GeV}$	HM	0	0.3 ± 0.05
		LM	0	1.8 ± 0.4
	$10 \text{ GeV} < \Delta m < 30 \text{ GeV}$	HM	0	0.7 ± 0.05
		LM	0	1.5 ± 0.4
	$30 \text{ GeV} < \Delta m < 80 \text{ GeV}$	HM	4	4.5 ± 1.5
		LM	0	1.7 ± 0.5
	$80 \text{ GeV} < \Delta m < 180 \text{ GeV}$	HM	3	4.6 ± 1.6
		LM	0	1.3 ± 0.4

Table 2: Remaining numbers of events after all cuts for sleptons, charginos and neutralinos. There are large correlations among both the selected events and expected background in the different analyses.

3.2.2 $\tilde{\chi}_1^0\tilde{\chi}_1^0$ Production with $\tilde{\ell}$ NLSP and $\tilde{\ell}^+\tilde{\ell}^-$ with $\tilde{\tau}$ NLSP

With a $\tilde{\ell}$ NLSP, the large neutralino pair production cross-section may make the 4-lepton plus missing energy signature $e^+e^- \rightarrow \tilde{\chi}_1^0\tilde{\chi}_1^0 \rightarrow \tilde{\ell}\tilde{\ell}'\tilde{\ell}'\tilde{\ell} \rightarrow (\ell^+\ell^-\tilde{G})(\ell'^+\ell'^-\tilde{G})$ the GMSB discovery channel. Because the scalar tau lepton may be the lightest slepton, the signature may predominantly include tau leptons. The selection is sensitive to all 4-lepton plus missing energy final states. Additionally, with a $\tilde{\tau}$ NLSP, if the neutralinos are too heavy to be produced and the scalar tau lepton is significantly lighter than the scalar electron and muon, then the 6-lepton plus missing energy final state may contribute via $e^+e^- \rightarrow \tilde{\ell}^+\tilde{\ell}^- \rightarrow (\ell^+\tilde{\tau}\tau)(\ell^-\tilde{\tau}\tau) \rightarrow (\ell^+\tau^+\tau^-\tilde{G})(\ell^-\tau^+\tau^-\tilde{G})$.

The analyses select low multiplicity events by allowing at most 10 tracks. The events are required to have significant missing energy by applying cuts on ϕ_{acop} , $\cos\theta_{\text{miss}}$, $p_T^{\text{miss}}/E_{\text{beam}}$ and E_{vis}/\sqrt{s} , listed in Table 3. In the 4-lepton analysis, we require two identified, isolated leptons in the event and remove Standard Model $\tau^+\tau^-\gamma$ events by vetoing events with photons with more than half the beam energy. In the 6-lepton analysis, only one identified, isolated lepton is required. This is because these events typically have only two high energy leptons, both taus, and they often have nearby tracks from the other decay products and are therefore not isolated. If the event is consistent with one lepton plus two hadronic jets an additional veto on $e^+e^- \rightarrow W^+W^- \rightarrow q\bar{q}\ell\nu$ is applied: events are removed if the invariant mass of the most energetic lepton and missing momentum is greater than 60 GeV, or if the mass of the two hadronic jets is greater than 60 GeV. Examples distributions of the event transverse momentum and the number of identified, isolated leptons are shown in Figure 2. The selection results are summarized in Table 4, and the numbers of selected events are consistent with Standard Model

Channel	ϕ_{acop}	$ \cos \theta_{\text{miss}} $	$p_T^{\text{miss}}/E_{\text{beam}}$	E_{vis}/\sqrt{s}
$\tilde{\chi}_1^0 \tilde{\chi}_1^0$	$> 10^\circ$	< 0.90	> 0.10	$[0.10, 0.90]$
$\ell^+ \ell^-$	–		> 0.12	$[0.10, 0.80]$

Table 3: *Analysis requirements on quantities used in the different $\tilde{\ell}$ or $\tilde{\tau}$ NLSP selections.*

Channel	data	bkg.
$\tilde{\chi}_1^0 \tilde{\chi}_1^0 \rightarrow (\ell \ell \tilde{G})(\ell' \ell' \tilde{G})$	2	1.9 ± 0.2
$\tilde{\ell}^+ \tilde{\ell}^- \rightarrow (\ell^+ \tau \tau \tilde{G})(\ell^- \tau \tau \tilde{G})$	5	5.2 ± 0.4

Table 4: *The numbers of events remaining after all cuts in the search for neutralinos and sleptons with a $\tilde{\ell}$ NLSP.*

sources.

The detection efficiencies for events from $\tilde{\chi}_1^0 \tilde{\chi}_1^0$ pair production assuming the decays $\tilde{\chi}_1^0 \rightarrow \tilde{\ell} \ell \rightarrow \ell \ell \tilde{G}$ are fairly uniform for different $\tilde{\chi}_1^0$ and $\tilde{\ell}$ masses, and about 50% if the neutralino decays into all three slepton generations with equal branching ratios, and 35% if it decays via staus with 100% branching ratio. The detection efficiencies for events from selectron and smuon pair production assuming decays into staus are also fairly uniform for different sparticle masses, and are typically about 50%.

4 Systematic Errors and Corrections

Systematic errors on the number of expected signal events arise from the following sources: the measurement of the integrated luminosity (0.5%); Monte Carlo statistics for the signal samples (1–2%), and interpolation errors when determining the efficiencies at arbitrary masses (typically 5%); gaugino field content of the $\tilde{\chi}^\pm$ and $\tilde{\chi}^0$ which can lead to different production and decay angular distributions ($< 5\%$); modelling of the cut variables in the Monte Carlo simulations (5–10%). The cut variable modelling error is determined by shifting each cut by an amount estimated by comparing data and Monte Carlo in high statistics samples.

The systematic errors on the expected number of background events are determined from: Monte Carlo statistics in the simulated background events (typically 5%); modelling of the cut variables (from 10–20%, depending on the analysis and kinematic region).

In the analyses in Sections 3.1.2 and 3.2.2, a common veto on energy deposition in the forward detectors was applied in the preselection. The rate of events in which accidental energy depositions in the forward detectors exceeds the veto thresholds used in the preselection is estimated from luminosity weighted random beam crossing events to be 2.9%. Since this effect is not included in the Monte Carlo simulations, the luminosity is reduced accordingly by this factor when deriving limits using the data.

5 Results

No significant excesses are observed in any channels, so limits are derived using the search results. Limits are derived using the method from Reference [26], including the effects of

systematic errors on the signal detection efficiencies and background expectation using the method from Reference [27].

5.1 Model Independent Interpretations

For a $\tilde{\chi}_1^0$ NLSP, assuming the prompt decay $\tilde{\chi}_1^0 \rightarrow \gamma \tilde{G}$, production cross-section limit contours are calculated in the mass plane of the particle produced *vs.* the mass of the $\tilde{\chi}_1^0$. In this scenario, limits on the production cross-sections for the processes $e^+e^- \rightarrow \tilde{\mu}^+\tilde{\mu}^-$, $e^+e^- \rightarrow \tilde{\tau}^+\tilde{\tau}^-$, $e^+e^- \rightarrow \tilde{\chi}_1^+\tilde{\chi}_1^-$ and $e^+e^- \rightarrow \tilde{\chi}_2^0\tilde{\chi}_1^0$ are shown in Figure 3. Typically, production cross-sections in excess of about 0.03 – 0.1 pb are excluded at the 95% confidence level.

For a $\tilde{\ell}$ NLSP, assuming the prompt decay $\tilde{\ell} \rightarrow \ell \tilde{G}$, production cross-section limit contours can be calculated in the mass plane of the particle produced *vs.* the mass of the $\tilde{\ell}$, shown in Figure 4. Typically, cross-sections for $e^+e^- \rightarrow \tilde{\chi}_1^0\tilde{\chi}_1^0$ larger than 0.05 – 0.06 pb are excluded at the 95% confidence level for the degenerate slepton case, while cross-section larger than 0.07 – 0.15 pb are excluded for the stau NLSP case. For scalar electron or muon pair production with a scalar tau NLSP, the cross-section limits are typically 0.06 – 0.13 pb.

5.2 GMSB Model Dependent Interpretations

While there is no single GMSB model, there are typically [1, 2, 3] six new parameters in addition to those of the SM:

$$F, \Lambda, M, N, \tan\beta \text{ and } \text{sign}(\mu). \quad (1)$$

The intrinsic SUSY breaking scale is \sqrt{F} , which also determines the \tilde{G} mass according to $m_{\tilde{G}} \simeq 2.5 \times F/(100 \text{ TeV})^2 \text{ eV}$. Since \sqrt{F} affects primarily the lifetime of the NLSP we do not vary it for this paper, but simply assume that this lifetime is short enough to have no effect on our detection efficiencies. The parameter Λ sets the overall mass scale for SUSY particles, M is the mass of the messenger particles, N is the number of sets³ of messenger particles, and $\tan\beta$ is the usual ratio of the Higgs vacuum expectation values. The final parameter is just the sign of the Higgs sector mixing parameter, μ , which introduces a two-fold ambiguity (the magnitude of μ is calculable from the other parameters in the minimal model by imposing radiative electroweak symmetry breaking). The messenger scale gaugino masses can be calculated using the relation

$$M_i = N \frac{\alpha_i}{4\pi} \Lambda g(\Lambda/M), \quad (2)$$

where the index i refers to the $U(1)$, $SU(2)$ or $SU(3)$ gauge group, and the α_i are the SM gauge couplings. The function $g(\Lambda/M)$ is always slightly greater than 1, but its effect is only significant when $\Lambda \approx M$. It is also possible to calculate all of the messenger scale scalar SUSY particle masses using Λ and N via

$$m^2 = 2 N \Lambda^2 f(\Lambda/M) \sum_{i=1}^3 k_i \left(\frac{\alpha_i}{4\pi} \right)^2, \quad (3)$$

³ N is technically the Dynkin index of the gauge representation of the messenger fields. To preserve gauge coupling unification, the messengers are assumed to form a GUT representation. In the simplest form, each of the N messenger particle sets has the quantum numbers of an $\mathbf{5} + \bar{\mathbf{5}}$ of $SU(\mathbf{5})$. The maximum number of messengers can be bounded by requiring the gauge interactions remain perturbative up the GUT scale, although this bound depends on M . For $M = 100 \text{ TeV}$, $N \leq 5$, while for $M = 10^{10} \text{ TeV}$, $N \leq 10$.

Parameter	Lower Value	Upper Value
$\tan \beta$	2	50
Λ	5 TeV	200 TeV
M	$1.01 \times \Lambda$	10^6 TeV
N	1	4
$\text{sign}(\mu)$	-1	+1

Table 5: *Parameter ranges considered in GMSB scans.*

where k_i are multiplicative factors determined by the particle's SM charge, hypercharge and colour charge. The function $f(\Lambda/M)$ is usually near 1, except when $\Lambda \approx M$. The electroweak scale particle masses may be calculated from the messenger scale masses using the renormalization group equations.

We will work in a theoretical framework based on Reference [1], extending it by including a full mass treatment for all three generations of sparticles. The theoretical calculations are embedded in the SUSYGEN [11] generator. The complete interpretation framework is described in Reference [28]. The SUSY breaking scale (or equivalently gravitino mass) is not considered explicitly in this section, although it is assumed that $M_{\tilde{G}} < 1$ GeV for the selection efficiencies to remain valid. The values of the parameters considered in our scan are shown in Table 5.

In Figure 5, 95% C.L. exclusion limits in the Λ *vs.* $\tan \beta$ plane are shown for different values of N . The $\tilde{\chi}_1^0$ NLSP signatures tend to be dominant for small N and low $\tan \beta$, while the $\tilde{\ell}$ NLSP signatures are more important for either larger N or larger $\tan \beta$. Absolute 95% C.L. lower limits on Λ of 48, 31, 22 and 19 TeV are established for $N = 1, 2, 3$ and 4, respectively. In Figure 6(a), the excluded region in the $M_{\tilde{\ell}}$ *vs.* $M_{\tilde{\chi}_1^0}$ plane is shown for $\tan \beta = 2$, corresponding to the case where the three sleptons are degenerate in mass. The dominant exclusion channels in the minimal model are $\tilde{\chi}_1^0 \tilde{\chi}_1^0 \rightarrow \gamma \tilde{G} \gamma \tilde{G}$ and $\tilde{\ell}^+ \tilde{\ell}^- \rightarrow \ell^+ \tilde{G} \ell^- \tilde{G}$. In Figure 6(b), the excluded region in the $M_{\tilde{\tau}}$ *vs.* $M_{\tilde{\chi}_1^0}$ plane is shown for $\tan \beta = 20$, corresponding to the case where the $\tilde{\tau}$ is significantly lighter than the other sleptons. The $\tilde{\chi}_1^0 \tilde{\chi}_1^0 \rightarrow \gamma \tilde{G} \gamma \tilde{G}$ channel remains powerful in this case, but the light $\tilde{\tau}$ means that only the $\tilde{\tau}^+ \tilde{\tau}^- \rightarrow \tau^+ \tilde{G} \tau^- \tilde{G}$ channel contributes to the significance from lepton pair final states.

Finally, 95% C.L. limits can be derived on the NLSP mass of $M_{\tilde{\ell}} > 83$ GeV and $M_{\tilde{\chi}_1^0} > 85$ GeV for $\tan \beta = 2$, and $M_{\tilde{\tau}} > 69$ GeV, $M_{\tilde{e}, \tilde{\mu}} > 88$ GeV and $M_{\tilde{\chi}_1^0} > 76$ GeV for $\tan \beta = 20$.

6 Conclusion

We have searched for signatures expected in models with gauge mediated SUSY breaking at a centre-of-mass energy of $\sqrt{s} = 189$ GeV with the OPAL detector at LEP. No evidence in any search channel over the expectations from the Standard Model was observed. Limits are placed on the production cross-sections for a number of processes for the prompt decays of the next-to-lightest SUSY particle to a gravitino. The results are used to constrain minimal models of gauge mediated supersymmetry breaking.

7 Acknowledgements

We particularly wish to thank the SL Division for the efficient operation of the LEP accelerator at all energies and for their continuing close cooperation with our experimental group. We thank our colleagues from CEA, DAPNIA/SPP, CE-Saclay for their efforts over the years on the time-of-flight and trigger systems which we continue to use. In addition to the support staff at our own institutions we are pleased to acknowledge the

Department of Energy, USA,

National Science Foundation, USA,

Particle Physics and Astronomy Research Council, UK,

Natural Sciences and Engineering Research Council, Canada,

Israel Science Foundation, administered by the Israel Academy of Science and Humanities,

Minerva Gesellschaft,

Benozzi Center for High Energy Physics,

Japanese Ministry of Education, Science and Culture (the Monbusho) and a grant under the Monbusho International Science Research Program,

Japanese Society for the Promotion of Science (JSPS),

German Israeli Bi-national Science Foundation (GIF),

Bundesministerium für Bildung und Forschung, Germany,

National Research Council of Canada,

Research Corporation, USA,

Hungarian Foundation for Scientific Research, OTKA T-029328, T023793 and OTKA F-023259.

References

- [1] S. Dimopoulos, S. Thomas, J.D. Wells, Nucl. Phys. B488 (1997) 39.
- [2] S. Ambrosanio, G.D. Kribs, S.P. Martin, Phys. Rev. D56 (1997) 1761.
- [3] G.F. Giudice, R. Rattazzi, “Theories with Gauge-Mediated Supersymmetry Breaking”, Phys. Rept. 322 (1999) 419-499 and Phys. Rept. 322 (1999) 501.
- [4] OPAL Collaboration, G. Abbiendi *et al.*, Eur. Phys. J. C14 (2000) 51.
- [5] OPAL Collaboration, G. Abbiendi *et al.*, “Photonic Events with Missing Energy in e^+e^- Collisions at $\sqrt{s} = 189$ GeV”, CERN-EP-2000-050, submitted to Eur. Phys. J. C.
- [6] OPAL Collaboration, G. Abbiendi *et al.*, Eur. Phys. J. C14 (2000) 187.
- [7] OPAL Collaboration, K. Ackerstaff *et al.*, Phys. Lett. B433 (1998) 195.
- [8] ALEPH Collaboration, R. Barate *et al.*, Eur. Phys. J. C16 (2000) 71.
- [9] DELPHI Collaboration, P. Abreu *et al.*, Eur. Phys. J. C16 (2000) 211.
- [10] OPAL Collaboration, K. Ahmet *et al.*, Nucl. Instr. Meth. A305 (1991) 275;
S. Anderson *et al.*, Nucl. Instr. Meth. A403 (1998) 326;
B.E. Anderson *et al.*, IEEE Trans. on Nucl. Science 41 (1994) 845;
G. Aguillion *et al.*, Nucl. Instr. Meth. A417 (1998) 266.

- [11] S. Katsanevas and P. Morawitz, *Comp. Phys. Comm.* 112 (1998) 227.
- [12] C. Dionisi *et al.*, in ‘Physics at LEP2’, eds. G. Altarelli, T. Sjöstrand and F. Zwirner, CERN 96-01, vol.2 (1996) 337.
- [13] T. Sjöstrand, *Comp. Phys. Comm.* 39 (1986) 347;
T. Sjöstrand, PYTHIA 5.7 and JETSET 7.4 Manual, CERN-TH 7112/93.
- [14] E. Boudinov *et al.*, ‘ $\gamma\gamma$ Event Generators’, hep-ph/9512371, Dec. 1995, and in ‘Physics at LEP2’, eds. G. Altarelli, T. Sjöstrand and F. Zwirner, CERN 96-01, vol.2 (1996) 187.
- [15] G. Marchesini *et al.*, *Comp. Phys. Comm.* 67 (1992) 465.
- [16] J.A.M. Vermaseren, *Nucl. Phys.* B229 (1983) 347.
- [17] Program KORALW V1.33, M. Skrzypek *et al.*, *Comp. Phys. Comm.* 94 (1996) 216;
M. Skrzypek *et al.*, *Phys. Lett.* B372 (1996) 286.
- [18] J. Fujimoto *et al.*, *Comp. Phys. Comm.* 100 (1997) 128.
- [19] S. Jadach, B. F. L. Ward, Z. Wąs, *Comp. Phys. Comm.* 79 (1994) 503.
- [20] S. Jadach, W. Płaczek, B.F.L. Ward, *Phys. Lett.* B390 (1997) 298.
- [21] D. Karlen, *Nucl. Phys.* B289 (1987) 23.
- [22] J. Allison *et al.*, *Nucl. Instr. Meth.* A317 (1992) 47.
- [23] OPAL Collaboration, K. Ackerstaff *et al.*, *Eur. Phys. J.* C2 (1998) 213.
- [24] J.L. Lopez and D.V. Nanopoulos, *Mod. Phys. Lett.* A11 (1996) 2473; *Phys. Rev.* D55 (1997) 4450.
- [25] OPAL Collaboration, G. Abbiendi *et al.*, *Eur. Phys. J.* C12 (2000) 551-565
- [26] Formulae 28.40 in “Review of Particle Properties”, R.M. Barnett *et al.*, *Phys. Rev.* D54 (1996).
- [27] R.D. Cousins and V.L. Highland, *Nucl. Instr. Meth.* A 320 (1992) 331.
- [28] E. Duchovni, J. Ihmels, A. Wodecki, J. Kraskiewicz, “Decay State Signatures at LEP2 for the Supersymmetric Theories with Gauge Mediated Supersymmetry Breaking”, Weizmann Institute preprint WIS/09/00-June-DPP.

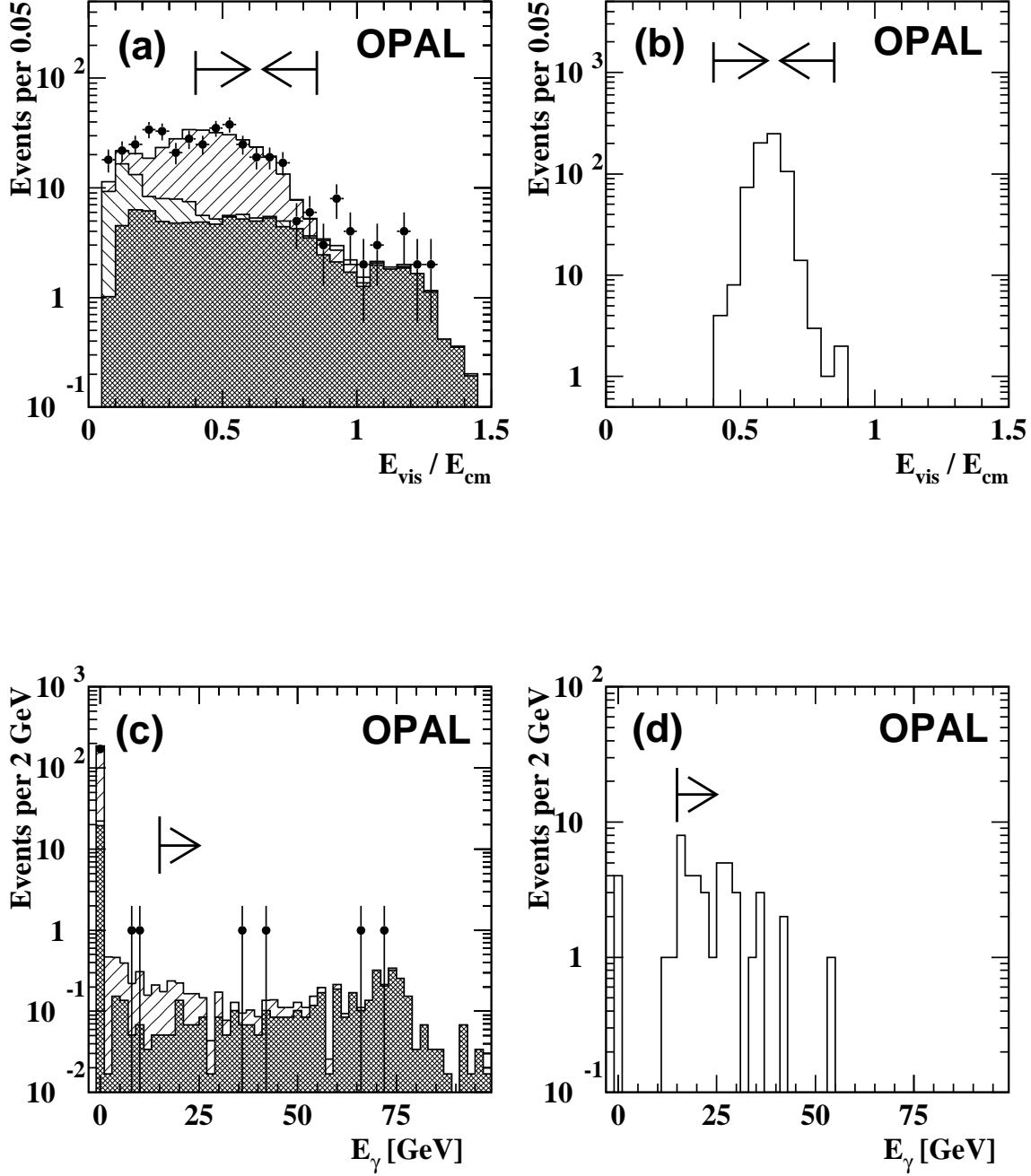


Figure 1: The distribution of the event visible energy, E_{vis} , and energy of the most energetic photon, E_γ , for events in the $\ell^+\ell^-\gamma\gamma$ analysis in Section 3.1.2. In (a) and (c) are shown the data (filled circles with error bars) and the prediction from different background processes, normalized to the acquired luminosity for the data: dilepton events (double hatched area), two-photon processes (negative slope hatching) and four-fermion processes (positive slope hatching). In (b) and (d) the prediction for simulated selectron events are shown for $m_{\tilde{e}} = 94$ GeV and with $m_{\tilde{\chi}_1^0} = 49$ GeV. The normalization of the signal distribution is arbitrary. The arrows indicate the region accepted by the analysis.

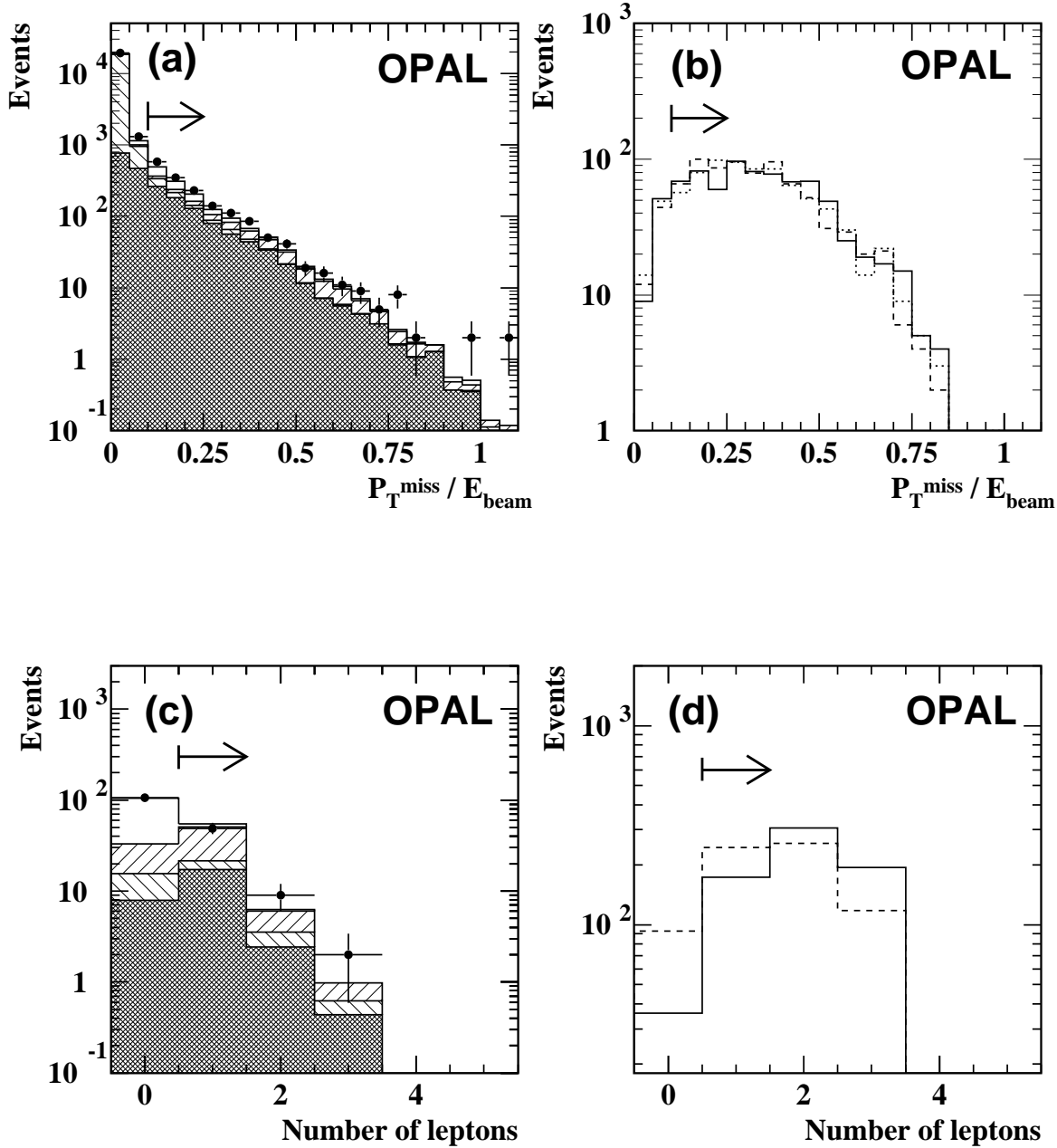


Figure 2: The event transverse momentum, p_T^{miss} , for events in the 4 leptons plus missing energy analysis after the preselection and requiring between 4 and 10 tracks for (a) data and Standard Model backgrounds (as for Figure 1) and (b) predictions from simulated neutralino events for $m_{\tilde{\ell}} = 50$ GeV and with $m_{\tilde{\chi}_1^0} = 60$ GeV (solid line), $m_{\tilde{\chi}_1^0} = 90$ GeV (dashed line) and with $m_{\tilde{\chi}_1^0} = 94$ GeV (dotted line), assuming equal branching fractions for all three lepton generations. Also shown are the distributions of the number of identified, isolated leptons after the missing energy cuts for events in the 6 leptons plus missing energy analysis for (c) data and Standard Model backgrounds (with an additional contribution from multihadronic events shown by the open area) and (d) scalar electron signal Monte Carlo with $m_{\tilde{e}} = 94$ GeV and with $m_{\tilde{\tau}} = 85$ GeV (solid line) and $m_{\tilde{\tau}} = 60$ GeV (dashed line). The normalizations of the signal distributions are arbitrary. The arrows indicate the region accepted by the analysis.

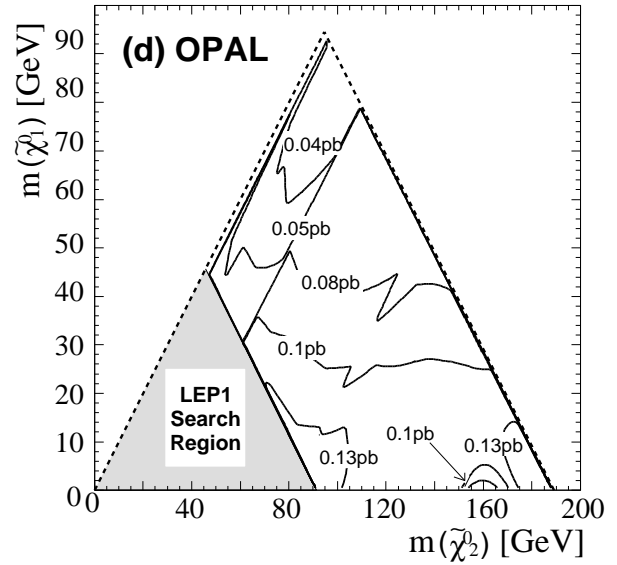
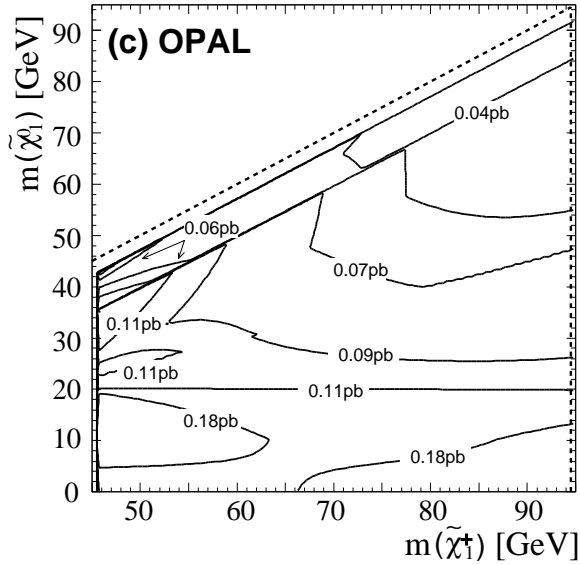
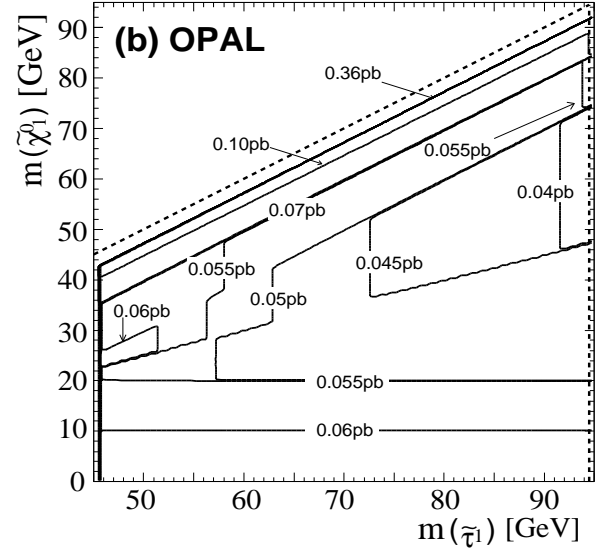
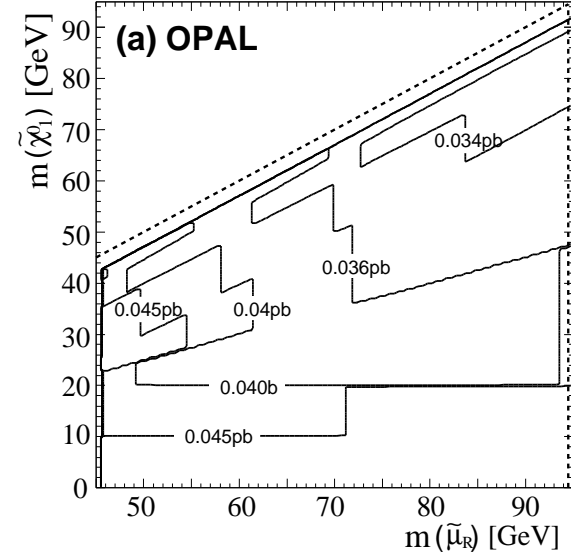


Figure 3: Limits at the 95% confidence level for the production cross-section of $e^+e^- \rightarrow$ (a) $\tilde{\mu}^+\tilde{\mu}^-$, (b) $\tilde{\tau}^+\tilde{\tau}^-$, (c) $\tilde{\chi}_1^+\tilde{\chi}_1^-$ and (d) $\tilde{\chi}_2^0\tilde{\chi}_1^0$, assuming decays via $\tilde{\chi}_1^0$ followed by the prompt decays $\tilde{\chi}_1^0 \rightarrow \gamma\tilde{G}$. The limits on $\tilde{e}^+\tilde{e}^-$ are essentially identical to those for $\tilde{\mu}^+\tilde{\mu}^-$. The dashed lines indicate the kinematic limit.

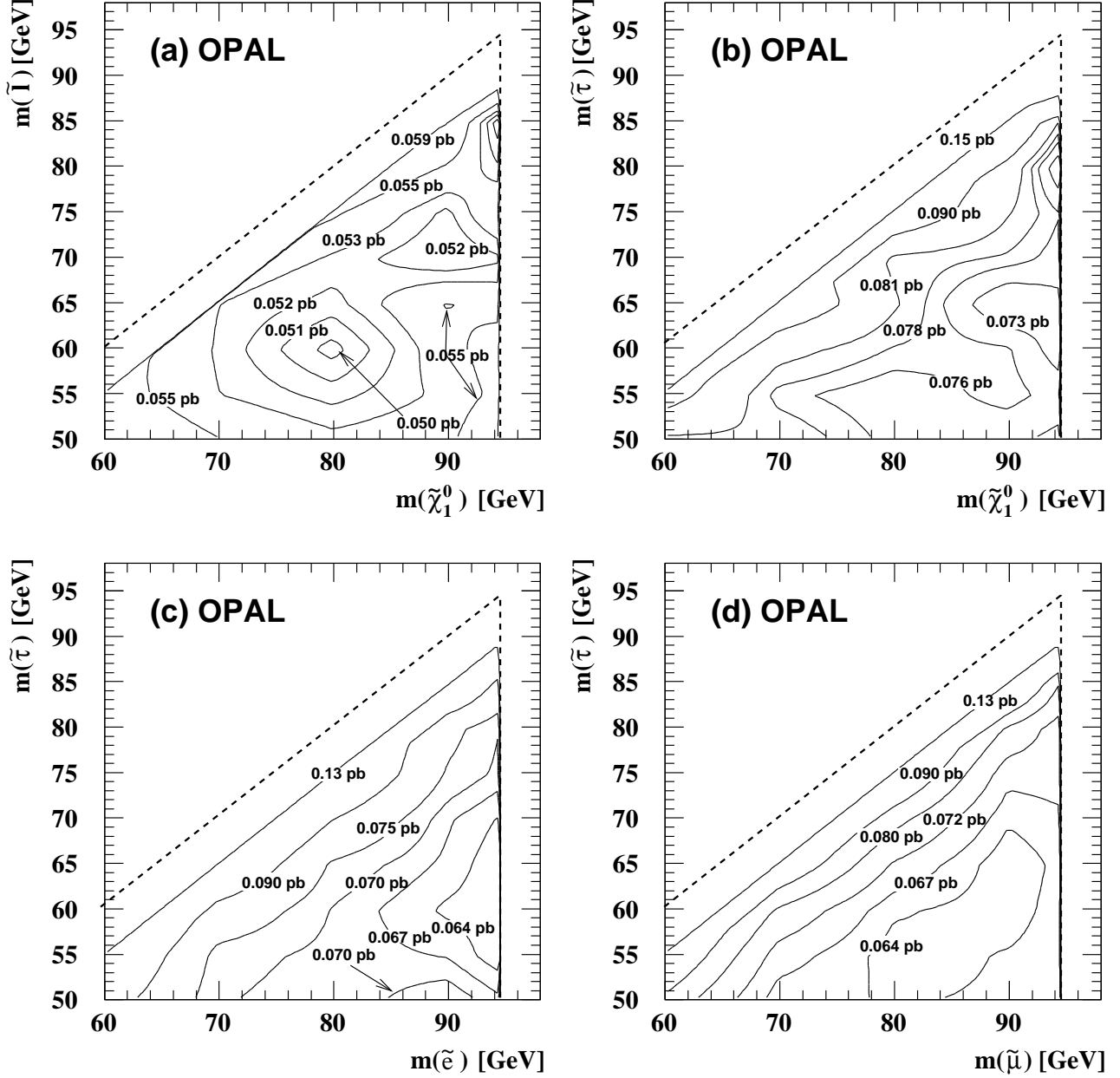


Figure 4: Limits at the 95% confidence level for the production cross-section of $e^+e^- \rightarrow$ (a) $\tilde{\chi}_1^0 \tilde{\chi}_1^0$ assuming the decays $\tilde{\chi}_1^0 \rightarrow \tilde{\ell} \ell$ with equal branching ratios to all three generations, (b) $\tilde{\chi}_1^0 \tilde{\chi}_1^0$ assuming the decays $\tilde{\chi}_1^0 \rightarrow \tilde{\tau} \tau$, (c) $\tilde{e}^+ \tilde{e}^-$ assuming the decays $\tilde{e} \rightarrow \tilde{\tau} \tau e$ and (d) $\tilde{\mu}^+ \tilde{\mu}^-$ assuming the decays $\tilde{\mu} \rightarrow \tilde{\tau} \tau \mu$. The limits assume that these decays are followed by the prompt decays $\tilde{\ell} \rightarrow \ell \tilde{G}$. The dashed lines indicate the kinematic limit.

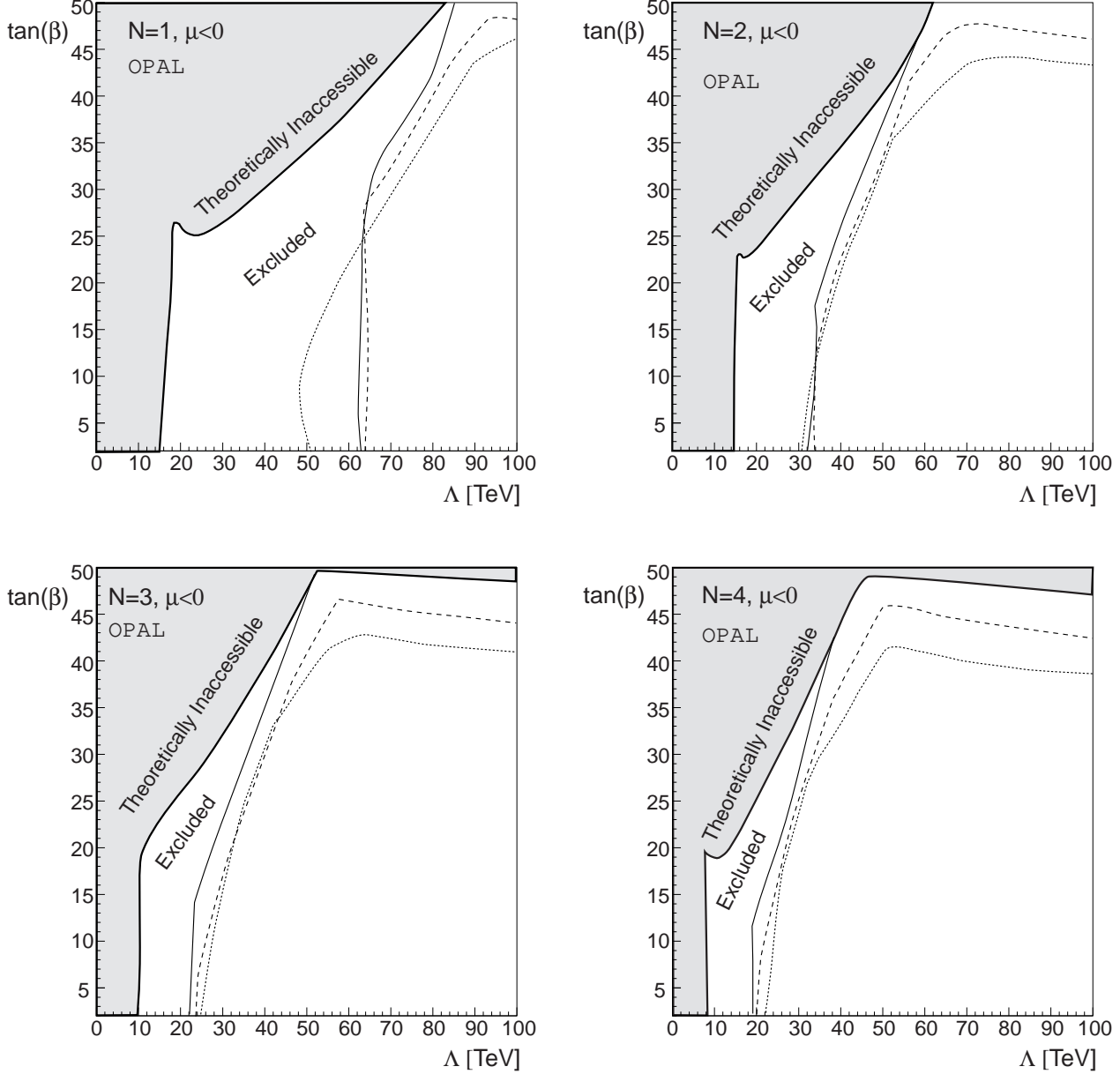


Figure 5: Excluded regions at the 95% C.L. in the Λ vs. $\tan\beta$ plane for $N = 1, 2, 3$ and 4 , and for $\mu < 0$. The areas above and to the left of the solid line are excluded for $M = 10^6$ TeV, the dashed line for $M = 250$ TeV, and the dotted line for $M = 1.01 \times \Lambda$. The shaded regions are theoretically inaccessible for $M = 10^6$ TeV (the inaccessible region is larger for smaller values of M). The exclusions for $\mu > 0$ are somewhat stronger.

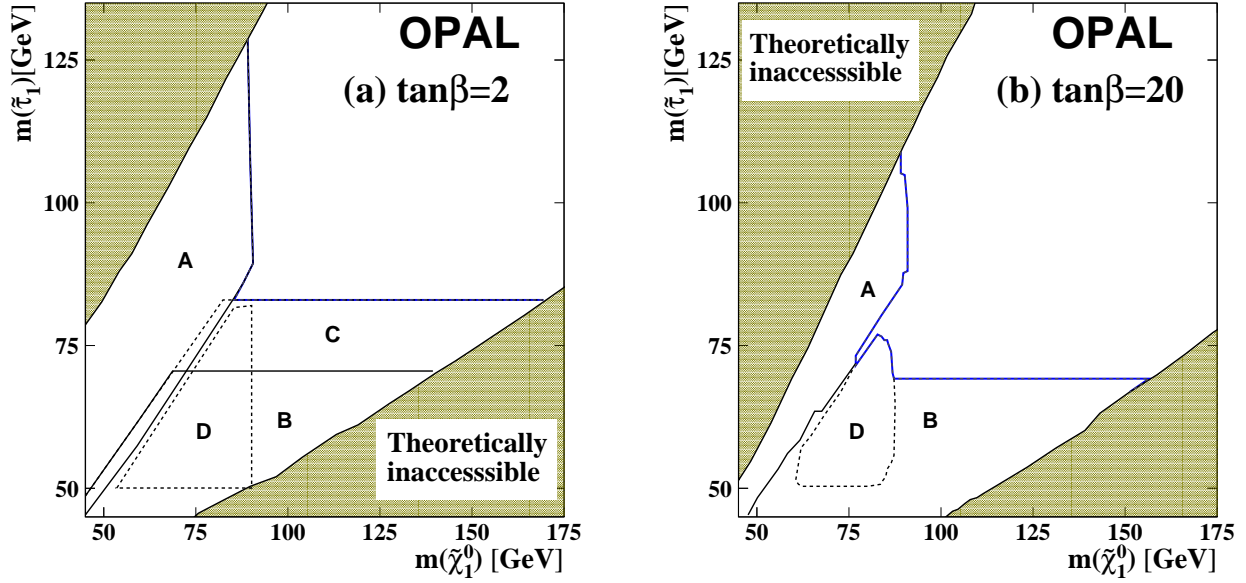


Figure 6: Excluded regions at the 95% C.L. in the $m_{\tilde{\ell}}$ vs. $m_{\tilde{\chi}_1^0}$ plane for (a) $\tan\beta = 2$ (approximately degenerate slepton case) and (b) $\tan\beta = 20$ (lighter stau case). Also shown are the regions exclusively excluded by (A) $\tilde{\chi}_1^0\tilde{\chi}_1^0 \rightarrow \gamma\tilde{G}\gamma\tilde{G}$, (B) $\tilde{\tau}^+\tilde{\tau}^- \rightarrow \tau^+\tilde{G}\tau^-\tilde{G}$, (C) $\tilde{\mu}^+\tilde{\mu}^- \rightarrow \mu^+\tilde{G}\mu^-\tilde{G}$ and (D) $\tilde{\chi}_1^0\tilde{\chi}_1^0 \rightarrow 4$ lepton final states. The other search channels do not contribute significantly to the exclusion regions in the minimal model. The shaded regions are theoretically inaccessible.